Nuclear Engineering and Technology 53 (2021) 3018–3025

Contents lists available at ScienceDirect

Nuclear Engineering and Technology

journal homepage: www.elsevier.com/locate/net

Original Article

A feasibility study of using a 3D-printed tumor model scintillator to verify the energy absorbed to a tumor

Tae Hoon Kim [a], Sangmin Lee [a], Dong Geon Kim [a], Jae Young Jeong [a], Hye Jeong Yang [b], Thomas Schaarschmidt [b], Sang Hyoun Choi [c], Gyu-Seok Cho [c], Yong Kyun Kim [a, **], Hyun-Tai Chung [d, *]

[a] Department of Nuclear Engineering, Hanyang University College of Engineering, Seoul, Republic of Korea
[b] Department of Biomedicine and Health Sciences & Biomedical Engineering, Catholic University College of Medicine, Seoul, Republic of Korea
[c] Research Team of Radiological Physics and Engineering, Korea Institute of Radiological & Medical Science, Seoul, Republic of Korea
[d] Department of Neurosurgery, Seoul National University College of Medicine, Seoul, Republic of Korea

ARTICLE INFO

Article history:
Received 14 August 2020
Received in revised form
30 March 2021
Accepted 31 March 2021
Available online 7 April 2021

Keywords:
3D-printed tumor model
Plastic scintillator
Absorbed energy
Volumetric dosimetry
Treatment planning system
Monte Carlo simulation

ABSTRACT

The authors developed a volumetric dosimetry detector system using in-house 3D-printable plastic scintillator resins. Three tumor model scintillators (TMSs) were developed using magnetic resonance images of a tumor. The detector system consisted of a TMS, an optical fiber, a photomultiplier tube, and an electrometer. The background signal, including the Cherenkov lights generated in the optical fiber, was subtracted from the output signal. The system showed 2.1% instability when the TMS was reassembled. The system efficiencies in collecting lights for a given absorbed energy were determined by calibration at a secondary standard dosimetry laboratory (k_{SSDL}) or by calibration using Monte Carlo simulations (k_{sim}). The TMSs were irradiated in a Gamma Knife® Icon™ (Elekta AB, Stockholm, Sweden) following a treatment plan. The energies absorbed to the TMSs were measured and compared with a calculated value. While the measured energy determined with k_{SSDL} was (5.84 ± 3.56) % lower than the calculated value, the energy with k_{sim} was (2.00 ± 0.76) % higher. Although the TMS detector system worked reasonably well in measuring the absorbed energy to a tumor, further improvements in the calibration procedure and system stability are needed for the system to be accepted as a quality assurance tool.

1. Introduction

Advanced radiosurgery uses sophisticated and complex equipment to deliver high radiation doses to tumors, which requires the precise verification of the amount and distribution of the radiation [1]. A treatment planning system (TPS) is used to develop an irradiation plan for a radiosurgery machine. The accuracy of these TPSs should be assessed as carefully as possible because it is a crucial factor determining treatment outcomes [2,3]. The Leksell GammaPlan® (LGP, Elekta AB, Stockholm, Sweden) is the TPS used for the Leksell Gamma Knife® (LGK, Elekta AB, Stockholm, Sweden) models Perfexion™ and ICON™. Upon the completion of treatment planning, the LGP calculates the values of several radiophysical quantities, such as point doses, the relative dose distribution, the mean, maximum, and minimum dose, and the energy absorbed to the tumor. The accuracies of these quantities are verified by point and planar dosimeters, such as ion chambers and radiochromic films at key locations. However, the energy absorbed to a tumor has not been measured and compared with the calculated value.

The absorbed energy is the quantity obtained by the integration of point doses over the tumor volume as follows:

$$E_T = \int_V dV\, D(\vec{r})\, \rho(\vec{r}) \quad (1)$$

where E_T is the energy absorbed to the tumor, V is the volume of the tumor, $D(\vec{r})$is the absorbed dose and $\rho(\vec{r})$ is the mass density

* Corresponding author. Seoul National University College of Medicine, Seoul, Republic of Korea.
** Corresponding author. Hanyang University College of Engineering, Seoul, Republic of Korea.
E-mail addresses: ykkim4@hanyang.ac.kr (Y.K. Kim), htchung@snu.ac.kr (H.-T. Chung).

https://doi.org/10.1016/j.net.2021.03.033

at $\vec{r}$. Some three-dimensional (3D) detectors, such as polymer gel dosimeters, have shown potential for treatment plan verification in 3D [4]. However, measuring absorbed energy using gel dosimeters is challenging because delineating a tumor in irradiated gel images is problematic. 3D printed plastic scintillator can be a solution. To measure E_T, a tumor model scintillator (TMS) can be fabricated in a tumor's shape and size using 3D printing with plastic resins. Plastic scintillators also have several advantages in measuring absorbed energy. Plastic scintillators have radiophysical properties similar to those of water. The light produced by the radiation exhibits a linear response to the absorbed energy and short decay times of several nanoseconds [5,6]. Most Compton electrons that generate visible lights are produced inside the scintillator such that the collected light is directly related to the absorbed energy in the detector. Because of its low cost, this approach is advantageous when developing a patient-specific detector. In this study, the authors measured the energy absorbed to a tumor using TMSs and compared this value with the value provided by LGP. Because the absorbed energy encompasses comprehensive 3D information regarding the calculated dose distribution, we could provide another criterion for the evaluation of LGP in addition to one- and two-dimensional dose verifications.

2. Materials and methods

2.1. TMS detector system

The TMSs used in this study were based on a vestibular schwannoma with a volume of 0.39 cm^3. The tumor delineated in the MR images was extracted to a stereolithography (STL) file and combined with a light guide using computer-aided design software (Fig. 1). The center of the mass of the tumor was aligned to the central axis of the light guide. Then, the TMS was printed by a commercial 3D printer (PICO2HD, ASIGA, Sydney, Australia) using in-house plastic scintillation resins [7]. The printing speed was approximately 20s per layer, and a TMS with a height of 11.5 mm was printed in less than an hour. The outer surface of the TMS was coated with reflective paint consisting of titanium dioxide (TiO_2) pigment (EJ-510, Eljen Technology, TX, USA) and black paint (M-07k, Gaianotes, Saitama, Japan). The paint coating was applied as uniformly as possible by dipping the TMS in the paint several times. The reflective paint and black paint thicknesses were approximately (0.5 ± 0.2) mm and (1.0 ± 0.3 mm), respectively.

The TMS was combined with an adapter to form a probe head (Fig. 2). The central axes of the TMS and the adaptor were on the same line. The adapter was fabricated with a photopolymer resin (3DKBLK, Carima, Seoul, Korea) using a 3D printer. Because the probe head was screwed onto a probe that encases an optical fiber, it could be exchanged with another probe head if necessary. Three probe heads with TMS and a dummy probe head were manufactured. A measurement system was established as shown in Fig. 2. The lights were transferred to a photomultiplier tube (PMT, H7422-40, Hamamatsu, Japan) using a 0.2 mm diameter silica core optical fiber (Thorlabs, Newton, NJ, US). The optical fiber with the highest commercially available numerical aperture, i.e., 0.5, was employed. The effective wavelength of the fiber ranged from 300 to 1200 nm. The light guide and optical fiber were connected without any auxiliary material between them. The fiber was combined with a PMT optical fiber adapter (A7412, Hamamatsu, Japan) using an FC-type connector. The PMT's output current was measured with a precision electrometer (6517B, Keithley, Ohio, USA). The PMT was automatically maintained at a constant temperature by monitoring the output of a thermistor installed nearby.

When measuring the light signal from the scintillator, undesired light signals can be generated in all optically transparent medium, which are caused by Cherenkov radiation [8]. The lights caused by Cherenkov radiation inside the scintillator constituted a few percent of the total produced lights. These lights were collected along with the scintillation lights and included in the calibration of the detector efficiencies. These lights did not impact the results because their intensity, which is similar to that of the scintillation lights, is proportional to the absorbed energy [9–11]. Because the current measured with the dummy head was a background current (I_{back}), including the Cherenkov radiation in the optical fiber, it was subtracted from the current measured with a TMS (I_{total}).

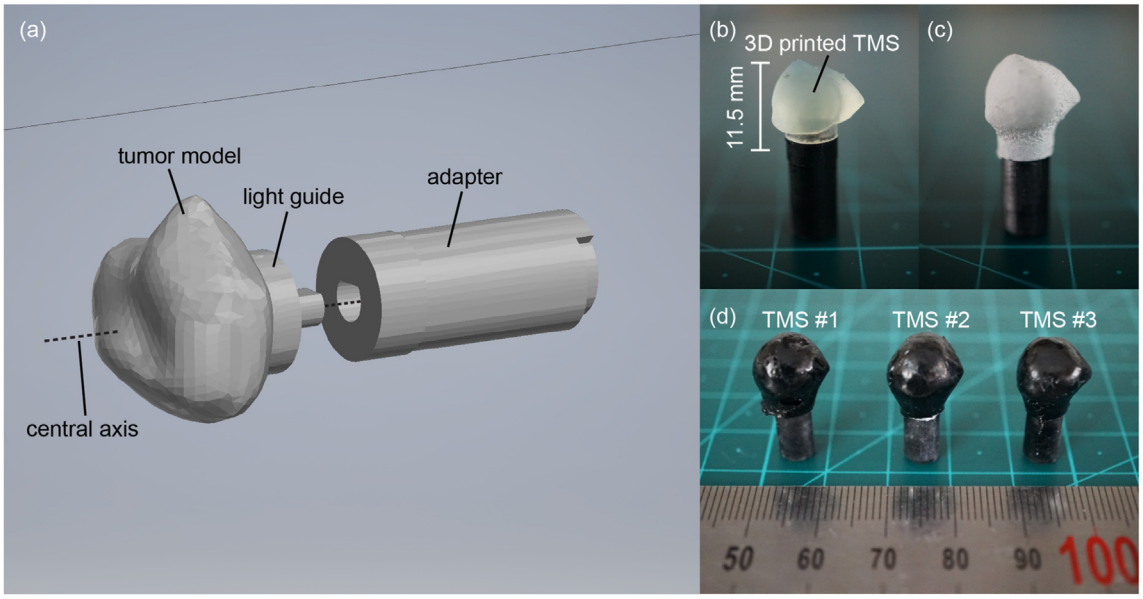

Fig. 1. (a) A schematic diagram of a probe head. The centers of the tumor and the light guide are located on the probe adapter's central axis. (b) A 3D-printed tumor model scintillator (TMS) combined with an adapter. (c) Reflective paint was uniformly coated on the TMS at a thickness of approximately 0.5 mm. (d) Black paint was coated over the reflector paint at a thickness of approximately 1 mm.

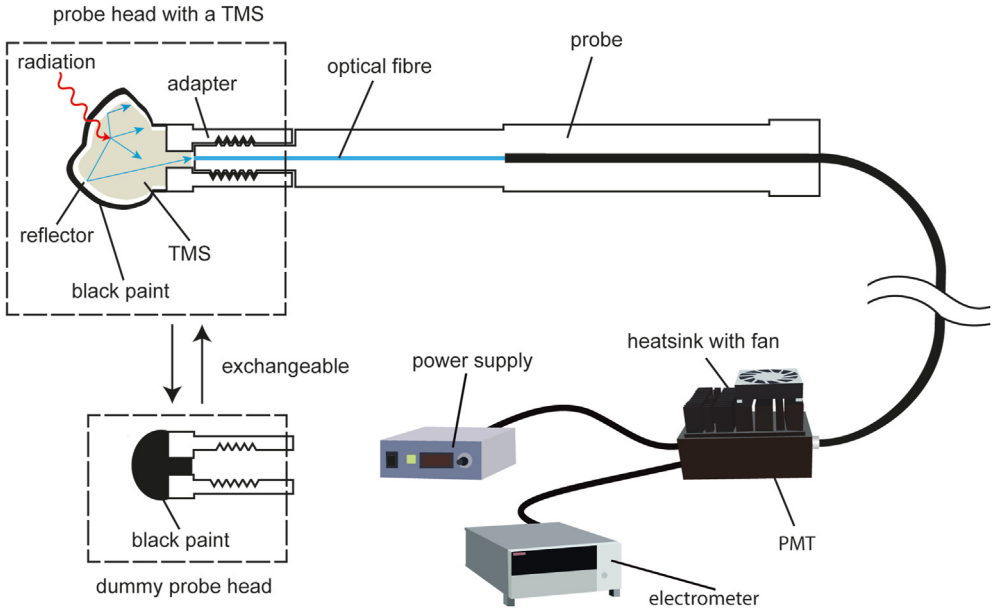

Fig. 2. The measurement system for a tumor model scintillator (TMS). The lights are collected using a photomultiplier tube (PMT) and converted into an electric signal. The probe heads are exchangeable such that a dummy probe head (probe head without a TMS) can be used to measure background signals, including Cherenkov radiation lights, from the optical fiber.

2.2. Calibration of the TMS system

The system calibration was performed in two ways. First, the relation between the measured charge and the energy absorbed to the TMS was determined at a secondary standard dosimetry laboratory (SSDL). The measurement conditions were set following a method similar to the standard protocol of ion chamber dosimetry. Second, a self-developed calibration using Monte Carlo (MC) simulation and an LGK was performed independently.

2.2.1. Calibration at an SSDL

The calibration coefficient of each TMS was determined at the Korea Institute of Radiological & Medical Sciences (KIRAMS), which is an SSDL organization. Consistent with the reference conditions given in the standard protocol for ion chambers, IAEA TRS 398, the center of the mass of a TMS was placed at a depth of 5 g/cm^2 inside a cubic water phantom of 30 cm × 30 cm × 30 cm [12]. The source-to-detector distance was 100 cm, and the field size of the cobalt 60 beams was 10×10 cm^2. The calibration coefficient was determined using eq. (2) as follows:

$$E_{SSDL} = k_{SSDL} \cdot M_{TMS} \tag{2}$$

where k_{SSDL} was the calibration coefficient determined at the SSDL, E_{SSDL} was the absorbed energy to water for a minute andM_{TMS} was the net charge accumulated for a minute. The output current was obtained for 100s, and the accumulated charge obtained between 30 and 90s was used in eq. (2) after background subtraction. E_{SSDL} was calculated by multiplying the absorbed dose at KIRAMS and the mass of water of the same volume as the TMS. The calibrations were performed using the three TMSs, and the k_{SSDL} of each detector was determined individually.

2.2.2. Calibration with Monte Carlo simulations

The MC code was written using Geant4 version 10.3 to simulate the LGK Icon model [13,14]. The simulation code and its verification have been described in another report [15]. In the simulation, the TMS's STL file was imported using the CADMesh interface (v1.1) and set at the center of the Elekta dosimetry phantom [16]. The rest of the geometry, including the TMS, was constructed as shown in Fig. 3 (a). Information regarding all materials used in the simulation is provided in Table 1. The Penelope low-energy electromagnetic physics model was used as a physics list, and the secondary particle production cut value was set to 990 eV, which was the minimum limit given in the physics list.

The calibration was determined in two steps. First, a factor converting the energy from the simulation to real absorbed energy to water was determined. A PTW 31010 ion chamber (PTW-Freiberg, Freiberg, Germany) was calibrated at an SSDL, i.e., Korea Research Institute of Standard and Science. The energy absorbed to water for a minute in a 16 mm collimator of LGK, $E_{meas,\ 31010}$, was measured with the chamber following the procedures described in IAEA TRS 483 [17]. The simulated absorbed energy per minute in the chamber, i.e., $\sum_{i=1}^{N_{31010}} E_{sim,31010}$, was obtained by an MC simulation assuming N_{31010} primary gamma rays were generated within a minute [18]. The energy conversion factor, k_E, was defined using eq. (3) as follows:

$$E_{meas,31010} = k_E \cdot \frac{\sum_{i=1}^{N_{31010}} E_{sim,31010}}{N_{31010}} \tag{3}$$

Then, the energy absorbed to a TMS for a minute, E_{sim}^{cali}, was obtained from the MC simulation of the TMS as follows:

$$\begin{aligned} E_{sim}^{cali} &= k_E \cdot \frac{\sum_{i=1}^{N_{TMS}} E_{sim,TMS}}{N_{TMS}} \\ &= \sum_{i=1}^{N_{TMS}} E_{sim,TMS} \cdot \frac{E_{meas,\ 31010}}{\sum_{i=1}^{N_{31010}} E_{sim,31010}} \cdot \frac{N_{31010}}{N_{TMS}} \end{aligned} \tag{4}$$

where $\sum_{i=1}^{N_{TMS}} E_{sim,\ TMS}$ was the simulated energy absorbed to the TMS with N_{TMS} primary gamma-rays per minute. Finally, the calibration coefficient based on the simulation (k_{sim}) was determined by eq. (5) as follows:

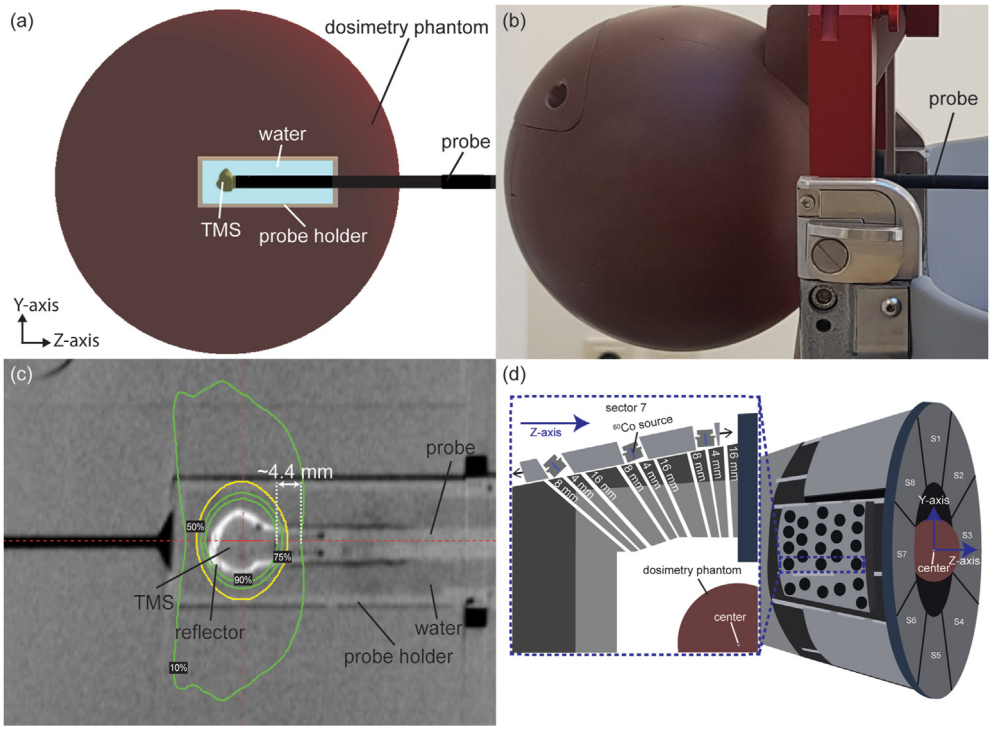

Fig. 3. (a) Geant4 simulation model of the tumor model scintillator (TMS) inside an Elekta dosimetry phantom. (b) The phantom with a probe holder was fixed to the patient couch of a Leksell Gamma Knife® (LGK) system. (c) A cone beam computed tomography image of the TMS system inside the phantom. Absorbed dose distributions (10%–90%) of the 16 mm collimator of an LGK are shown. (d) Schematic diagram of all LGK sectors (S1 − S8) and cross-section of sector 7 showing collimators (4, 8, 16 mm). The cobalt sources move back and forth such that different size collimators can be selected for each sector.

Table 1
Density and atomic mass fraction of the substances used in the Monte Carlo simulations.

Material	Density (g/cm^3)	Atomic mass fraction (%)							
		H	C	N	O	P	Cl	Ca	Ti
Water	1.00	11.2	–	–	88.8	–	–	–	–
Polymer resin[a] (probe and adapter)	1.15	5.7	67.9	26.4	–	–	–	–	–
TMS[b]	1.167	7.5	67.2	0.1	25.2	0.01	–	–	–
Reflector[c]	1.18	2.9	17.2	–	38.9	–	–	–	41.1
Black paint[d]	1.10	4.5	54.1	12.6	28.8				
Solid Water®[e]	1.04	8.0	67.2	2.4	19.9	–	0.1	2.3	–

[a] http://carima.com/.
[b] Tumor Model Scintillator. Values differ from those reported in a previous study (Son et al., 2018) due to modification.
[c] https://eljentechnology.com/images/products/data_sheets/EJ-510_EJ-520.pdf.
[d] http://www.inchem.org/documents/icsc/icsc/eics1272.htm.
[e] based on Gammex 457-CTG, by Gammex, Inc.

$$E_{sim}^{cali} = k_{sim} \cdot M_{TMS}^{cali} \quad (5)$$

where M_{TMS}^{cali} was the charge measured by the TMS in the LGK for a minute.

The measurements with the LGK were performed at the center of an Elekta dosimetry phantom (Elekta AB, Stockholm, Sweden) made with Solid Water® (Gammex RMI, Middleton, WI, USA). The TMS center was set at the phantom's center as shown in Fig. 3. The space inside the probe holder was filled with distilled water. Seven calibration shots with different combinations of collimators were composed to investigate the energy rate dependency. The compositions of the seven shots are described in Table 2. Linear fitting was performed to obtain k_{sim}. Since the net charge was used, the line's intercept was fixed to zero. The value of k_{sim} of each TMS was determined individually.

2.3. Absorbed energy measurement

As shown in Fig. 3 (c), cone beam computed tomography (CBCT) images of the TMS system placed inside the phantom were obtained. A LGK treatment plan consisting of nine shots (A1 − A9) was developed, and 8 Gy was prescribed at the 60% isodose line as shown in Fig. 4. The measured absorbed energy of each planned shot was obtained using k_{SSDL} or k_{sim}, and their sum was used as the measured energy absorbed to a TMS. The measured absorbed energy was compared with the energy calculated by LGP, $E_{LGP,w}$ or $E_{LGP,TMS}$. When a measured energy (E_{SSDL}) determined with k_{SSDL} was assessed, the energy absorbed to water ($E_{LGP,w}$) of the same volume and shape as a TMS was used because k_{SSDL} was determined using the energy absorbed to water at the SSDL. When a measured

Table 2
Collimator and sector configurations of the seven shots used for the detector calibration with the Monte Carlo simulation. Shots C1 – C3 used all sectors of the collimator (4, 8, and 16 mm) of an LGK Icon. Shots C4 – C7 were composed of the 16 mm collimator, but some of the eight sectors (S1 – S8) were blocked to obtain different absorbed energies per minute. The numbers (4, 8, or 16) in the sector configuration column indicate the size of the collimator, and B indicates a blocked sector.

Shot number	Sector configuration								Nominal dose rate (Gy/min)	E_{sim}^{cali}(μJ/min)
	S1	S2	S3	S4	S5	S6	S7	S8		
C1	4	4	4	4	4	4	4	4	1.948 ± 0.025	339.6 ± 4.4
C2	8	8	8	8	8	8	8	8	2.154 ± 0.028	882.2 ± 11.5
C3	16	16	16	16	16	16	16	16	2.393 ± 0.031	1172.4 ± 15.2
C4	16	B	B	B	B	B	B	B	0.299 ± 0.004	146.8 ± 1.9
C5	16	16	B	B	B	B	B	B	0.598 ± 0.008	293.5 ± 3.8
C6	16	16	16	16	B	B	B	B	1.197 ± 0.016	586.7 ± 7.6
C7	16	16	16	16	16	16	B	B	1.795 ± 0.025	879.8 ± 11.4

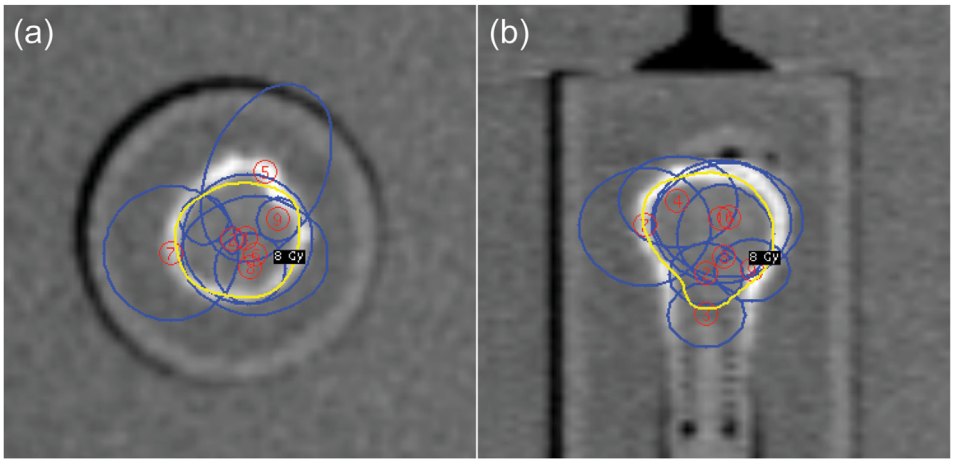

Fig. 4. Axial (a) and coronal (b) dose distributions of the treatment plan to irradiate a tumor model scintillator are shown in cone beam computed tomography images. The plan consisted of nine shots (blue lines, A1-A9), and 8 Gy were prescribed at the 60% isodose surface (yellow line). (For interpretation of the references to colour in this figure legend, the reader is referred to the Web version of this article.)

energy (E_{sim}) determined with k_{sim} was evaluated, $E_{LGP,TMS}$ was used as the calculated value, which was obtained by multiplying the mass density ratio of the TMS to $E_{LGP,w}$. All errors presented in this study are the standard deviation of the measured or calculated values unless stated otherwise.

3. Results

A TMS could be fabricated within a few hours. The masses of each TMS are shown in Table 3. The physical characteristics were measured with a cube printed with the same resin. The mass density was (1.167 ± 0.003) g/cm^3. The emission peak was 470 nm, and the light output was 21.1% of that of the commercial scintillator BC-408 (Saint-Gobain Crystals, Paris, France) [19]. The transmittance was (17.62 ± 4.94) %, the absorption length was (24.15 ± 4.42) cm, and the refractive index was (1.51 ± 0.01) at the peak wavelength.

When a probe head was irradiated with a 16 mm shot, the optical fiber section irradiated by more than 10% of the maximum energy was approximately 4.4 mm long as shown in Fig. 3 (c). The dummy detector's output current was (2.4 ± 0.1) % of the current from the TMS detector on average. The largest variation in the net current after reassembling the probe head and optical fiber was 2.1%, which was found using TMS #1.

According to the MC simulations, the absorbed energy decreased by (0.01 ± 0.19) % on average when a 0.5 mm thick reflector was added to the TMS. The absorbed energy increased by (0.11 ± 0.04) % on average when 1.0 mm thick black paint was applied over the reflector. These variations, however, did not affect the results of this study because these effects were embedded in the calibration.

On the day of the calibration at the SSDL, the dose rate of KIRAMS was (0.1780 ± 0.0018) Gy/min. The net charge accumulated for 1 min and the corresponding calibration coefficient are shown in Table 3. When the TMS detectors were calibrated with the MC simulation and an LGK, the dose rate was (2.393 ± 0.031) Gy/min.

Table 3
Calibration coefficients determined at a secondary standard dosimetry laboratory (k_{SSDL}) and by Monte Carlo simulations (k_{sim}) for each tumor model scintillator (TMS). k_{SSDL} should be multiplied by the mass density ratio of TMS (1.167) for comparison with k_{sim}.

TMS #	Mass (g)	Net charge at SSDL (μC)	Calibration coefficient	
			k_{SSDL} (J/C)	k_{sim} (J/C)
TMS #1	0.4913 ± 0.001	1.112 ± 0.005	67.77 ± 0.74	90.06 ± 1.39
TMS #2	0.4878 ± 0.001	1.454 ± 0.003	51.46 ± 0.53	62.70 ± 0.96
TMS #3	0.4955 ± 0.001	0.981 ± 0.003	76.30 ± 0.79	94.90 ± 1.45

The energy absorbed to the TMS of each calibration shot is shown in Table 2. The MC simulation of the seven calibration shots performed with 1 billion primary particles took less than 11h each with an 88 thread workstation. The measured currents (I_{total}, I_{back}) of the calibration shots are shown in Fig. 5 (a). Fig. 6 shows the results of the linear fittings performed to determine the k_{sim} of each TMS. The error bar along the horizontal axis is the standard deviation of the measured charge, and the error bar along the vertical axis is the statistical uncertainty of the simulation. The error bars have sizes similar to those of the symbols in Fig. 6. The adjusted R^2 values of the fittings were 0.99952, 0.99953, and 0.99955. The values of k_{sim} are presented in Table 3. To compare the two types of calibration coefficients, k_{SSDL} should be multiplied by the mass density ratio of TMS to water (1.167).

The output currents of the planned shots are shown in Fig. 5 (b). The control software of the LGK automatically arranged the shot order in Fig. 5 (b). The measured absorbed energy, i.e., the sum of the nine plan shot energies, is shown in Table 4. The measured energy errors of each TMS are the combined errors of the calibration error and the charge measurement errors. The calibration error was 1.05% for the E_{SSDL}, which was provided by the SSDL. The error of the simulation-based calibration was 1.53%, which was the combined values of the LGK dose rate uncertainties and linear fitting uncertainties. The planned shots' charge measurement errors were the standard deviation of each measurement and were 1.35%, 0.61%, and 0.88% for TMS1, 2, and 3, respectively. LGP provided the errors of the calculated energies, but the definitions are not described. While E_{sim} was (2.00 ± 0.76) % larger than the calculated energy, E_{SSDL} was (5.84 ± 3.56) % smaller.

4. Discussion

This study showed that the TMS system could measure the energy absorbed to a tumor with a few percent difference from the value provided by LGP. Verification of the absorbed energy can be used as an additional criterion for assessing a TPS and can be clinically meaningful because the number of DNA aberrations in a tumor is positively associated with the absorbed energy [20]. Although the minimum dose or the prescription dose is more likely a predictive factor of tumor control or complications, these values have not been experimentally verified over a whole tumor. The authors could assess the accuracy of the calculated energy absorbed to a tumor, which is a radiophysical quantity encompassing three-dimensional information, using a TMS.

Because the TMS detector system is in the development stage, several aspects need to be improved. It is essential to obtain the absorbed energy of a given tumor consistently. In this study, the variation, i.e., one standard deviation, was 3.8% in E_{SSDL} and 0.7% in E_{sim}. TMS #1 showed more substantial discrepancies than the others. The authors assume that this difference occurred because TMS #1 was printed first and underwent wear while repeating the preparatory measurements. TMS #2 and #3 were used for the main experiment immediately after printing and showed smaller variations of 0.9% and 0.5% in E_{SSDL} and E_{sim}, respectively. The main reason for the discrepancy among the calibration factor of TMSs was the different contact surface conditions between the TMS and the optical fiber. The mass and shape of the 3D-printed scintillators also differed. The thickness and uniformity of the applied reflector and black paint also slightly varied. Although these differences among the TMSs could be handled to an acceptable range through calibrations, it would be desirable to obtain consistent calibration coefficients for each TMS with a more stringent manufacturing process.

Calibrating a detector at an SSDL to verify the absolute value of the absorbed energy is ideal. In this study, the energies measured with the SSDL calibration showed a more significant difference from the calculated value, i.e., 5.84%, than those with the simulation-based calibration. However, we should not conclude that SSDL calibration is inferior to simulation-based calibration based on this result since some errors were evitable. While the authors did not reassemble the TMS probe head between the simulation-based calibration and the planned shot irradiation, the TMS probe heads were reassembled once in SSDL calibrations. The decoupling and recoupling of the TMS could be avoided if the authors measured with a dummy probe head before the measurement with the TMS probe head at the SSDL and after the TMS measurement at the LGK site. Another source of error was the angular dependence of k_{SSDL}. Since the TMS shape was asymmetric, k_{SSDL} depended on the orientation of the TMS to the beam direction. k_{SSDL} should have been obtained at several angles but was only measured in a single direction. There was no angular dependence in k_{sim} because the 192-directional beams of the LGK were distributed symmetrically around the TMS. In the next step of this project, rotation dependence will be carefully evaluated, and reassembling will be avoided. One unavoidable error in the SSDL calibration was that only a single absorbed energy value was applied to the whole TMS volume. Although only small absorbed energy variations were expected inside the TMS, MC simulations are necessary to obtain the absorbed energy more accurately. The authors are developing an MC simulation code for the cobalt irradiator of the SSDL.

Suppose that we are interested only in assessing the energy calculation procedure of a TPS rather than the accuracy of the calculated value. In this case, it seems to be enough to use the simulation-based calibration and an LGK at each site because the

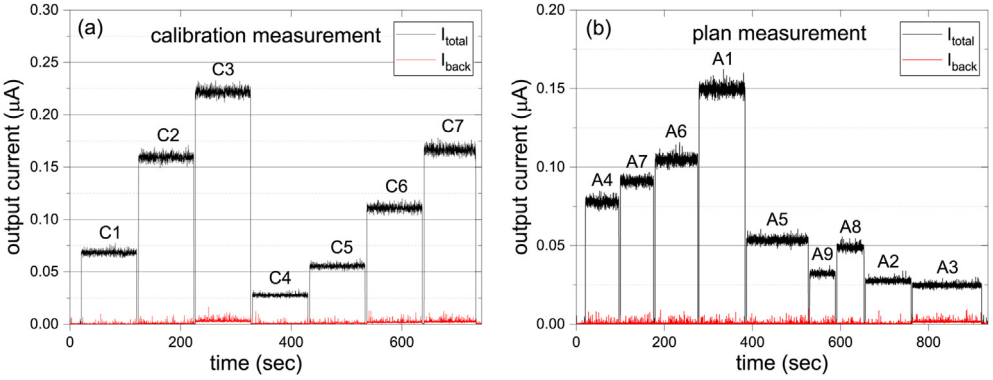

Fig. 5. (a) An example of the output currents (I_{total}) of seven calibration shots (C1–C7) measured with a tumor model scintillator. Background currents (I_{back}) were measured with a dummy probe head under the same conditions. (b) An example of the I_{total} and $I_{back}$of the nine planned shots (A1-A9).

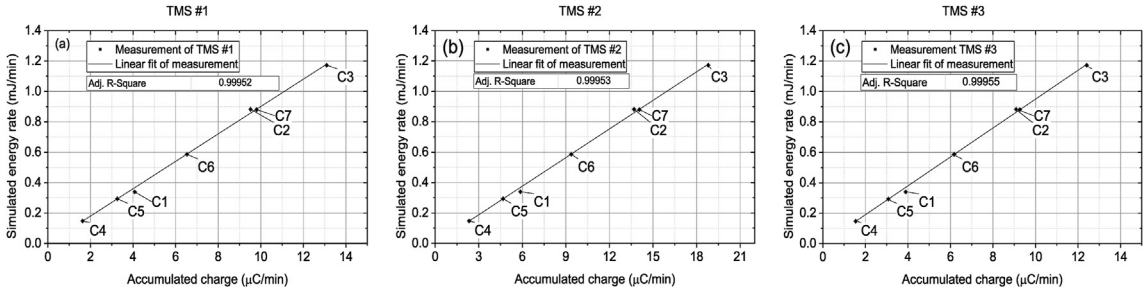

Fig. 6. Results of the linear fittings of the three tumor model scintillators (TMSs) to determine the simulation-based calibration coefficients. The horizontal axis shows the measured charge per minute, and the error bar is the standard deviation. The vertical axis is the energy absorbed to a TMS per minute obtained via Monte Carlo simulations.

Table 4
Comparison of the calculated and measured absorbed energies. E_{SSDL} is the measured energy absorbed to water of the same volume and shape as a tumor model scintillator (TMS). E_{SSDL} was obtained by calibration at a secondary standard dosimetry laboratory (SSDL). E_{sim} is the measured energy absorbed to a TMS obtained by calibration based on Monte Carlo simulation. $E_{LGP,w}$ is the energy absorbed to water provided by LGP under the assumption that the TMS is composed of water, and $E_{LGP,TMS}$ is the value obtained by multiplying the mass density ratio of the TMS (1.167) by $E_{LGP,w}$.

TMS #	Absorbed energy (mJ)			
	E_{SSDL}	$E_{LGP,w}$	E_{sim}	$E_{LGP,TMS}$
TMS #1	3.875 ± 0.067	–	5.148 ± 0.106	–
TMS #2	4.163 ± 0.050	–	5.072 ± 0.084	–
TMS #3	4.108 ± 0.056	–	5.110 ± 0.091	–
Mean	4.049 ± 0.153	4.30 ± 0.54	5.110 ± 0.038	5.01 ± 0.63

calibration and measurement are performed under the same conditions. The measured energy obtained with the simulation-based calibration was 2.00% higher than the calculated value. This difference was within the acceptable range of the absolute dose measurement of the LGK, which is a 3% difference. There were several sources of error in the simulation for calibration. First, the optical properties of the materials were not considered. While the center of the mass was irradiated in the calibration, various TMS locations were irradiated in the planned shot measurement. Because the relationship between the absorbed energy and the light output varies depending on the irradiation position, optical simulation should be included for better accuracy. In a separate measurement, it was found that the light output could increase 18% at the maximum when a 16-mm shot was irradiated near the TMS-fiber junction. The authors presumed that this effect could be smaller in a multi-shot plan in which the shots were distributed over a target, as shown in Fig. 4. An MC simulation code considering optical characteristics is under development. Second, the simulated absorbed energy distribution of a single collimator slightly differed from the radiochromic film measurements [15]. In the outer region, where the absorbed energy was smaller than approximately 20% of the maximum energy, more absorbed energy was measured than predicted by the simulation. This deviation was problematic when a 4 mm shot was irradiated for calibration since some TMS portion was in the area with deviation. For a 4 mm shot, more lights were collected than suggested by the simulation, which could explain the most substantial discrepancies between the 4 mm calibration shot (C1) and the fitted lines in Fig. 6. The discrepancy of C1 was (7.8 ± 0.3) % from the fitted value. Taking this account, it might be better to use different calibration coefficients for each collimator. Nevertheless, the authors employed a linear fitting method because a planned shot can have different size collimators at each sector, and it was impractical to determine the calibration coefficients of all possible combinations. When the calibration coefficients of the 4 mm and 8 mm shots were applied instead of the fitted values, E_{sim} became (5.112 ± 0.036) mJ, which was practically identical to the present value.

5. Conclusions

The energy absorbed to a tumor calculated from the treatment planning system for LGK radiosurgery was measured with a self-manufactured scintillation detector system for the first time. The measured energies showed differences from the calculated values of less than 6%. Although the TMS detector system worked reasonably in measuring the energy absorbed to a tumor, further improvements in the calibration procedure and system stability are needed for this approach to be accepted as a quality assurance tool.

Declaration of competing interest

The authors declare that they have no known competing financial interests or personal relationships that could have appeared to influence the work reported in this paper.

Acknowledgements

This study was supported by the Ministry of Science and ICT (grant numbers NRF-2016M2A2A6A03946564 and NRF-2020R1F1A1061144).

Appendix A. Supplementary data

Supplementary data to this article can be found online at https://doi.org/10.1016/j.net.2021.03.033.

References

[1] H.-T. Chung, D.G. Kim, Modern radiosurgery equipment for treating brain metastases, Current and Future Management of Brain Metastasis 25 (2012) 236–247.
[2] N. Agazaryan, T.D. Solberg, J.J. DeMarco, Patient specific quality assurance for the delivery of intensity modulated radiotherapy, J. Appl. Clin. Med. Phys. 4 (1) (2003) 40–50.
[3] J. Malicki, The importance of accurate treatment planning, delivery, and dose verification, Rep. Practical Oncol. Radiother. 17 (2) (2012) 63.
[4] J. Novotný Jr., P. Dvořák, V. Spěváček, J. Tintěra, J. Novotný, T. Čechák, R. Liščák, Quality control of the stereotactic radiosurgery procedure with the polymer-gel dosimetry, Radiother. Oncol. 63 (2) (2002) 223–230.
[5] S. Beddar, L. Archambault, N. Sahoo, F. Poenisch, G.T. Chen, M.T. Gillin, R. Mohan, Exploration of the potential of liquid scintillators for real-time 3D dosimetry of intensity modulated proton beams, Med. Phys. 36 (5) (2009) 1736–1743.
[6] L. Wootton, R. Kudchadker, A. Lee, S. Beddar, Real-time in vivo rectal wall dosimetry using plastic scintillation detectors for patients with prostate cancer, Phys. Med. Biol. 59 (3) (2014) 647.
[7] J. Son, D.G. Kim, S. Lee, J. Park, Y. Kim, T. Schaarschmidt, Y.K. Kim, Improved 3D printing plastic scintillator fabrication, J. Kor. Phys. Soc. 73 (7) (2018)

887–892.
[8] A. Beddar, T. Mackie, F. Attix, Cerenkov light generated in optical fibres and other light pipes irradiated by electron beams, Phys. Med. Biol. 37 (4) (1992) 925.
[9] J. Jelley, Cerenkov radiation and its applications, Br. J. Appl. Phys. 6 (7) (1955) 227.
[10] L. Archambault, A.S. Beddar, L. Gingras, R. Roy, L. Beaulieu, Measurement accuracy and Cerenkov removal for high performance, high spatial resolution scintillation dosimetry, Med. Phys. 33 (1) (2006) 128–135.
[11] G.F. Knoll, Radiation Detection and Measurement, John Wiley & Sons2010.
[12] P. Andreo, D.T. Burns, K. Hohlfeld, M.S. Huq, T. Kanai, F. Laitano, V. Smyth, S. Vynckier, Absorbed Dose Determination in External Beam Radiotherapy: an International Code of Practice for Dosimetry Based on Standards of Absorbed Dose to Water, Iaea Trs, 2000, p. 398.
[13] S. Agostinelli, J. Allison, K.a. Amako, J. Apostolakis, H. Araujo, P. Arce, M. Asai, D. Axen, S. Banerjee, G. Barrand, GEANT4—a simulation toolkit, Nucl. Instrum. Methods Phys. Res. Sect. A Accel. Spectrom. Detect. Assoc. Equip. 506 (3) (2003) 250–303.
[14] J. Allison, K. Amako, J. Apostolakis, H. Araujo, P.A. Dubois, M. Asai, G. Barrand, R. Capra, S. Chauvie, R. Chytracek, Geant4 developments and applications, IEEE Trans. Nucl. Sci. 53 (1) (2006) 270–278.
[15] T.H. Kim, T. Schaarschmidt, H.J. Yang, Y.K. Kim, K.J. Chun, Y. Choi, H.-T. Chung, Development of an IAEA phase-space dataset for the Leksell gamma Knife® Perfexion™ using multi-threaded Geant4 simulations, Phys. Med. 64 (2019) 222–229.
[16] C.M. Poole, I. Cornelius, J.V. Trapp, C.M. Langton, A cad interface for geant4, Australas, Phys. Eng. Sci. Med. 35 (3) (2012) 329–334.
[17] S. Vatnisky, A. Meghzifene, K. Christaki, H. Palmans, P. Andrew, M. Saiful Huq, Dosimetry of Small Fields Used in External Beam Radiotherapy: an International Code of Practice for Reference and Relative Dose Determination, International Atomic Energy Agency, 2017. IAEA TRS-483.
[18] T. Schaarschmidt, T.H. Kim, Y.K. Kim, H.J. Yang, H.-T. Chung, GEANT4-based Monte Carlo simulation of beam quality correction factors for the Leksell gamma Knife® Perfexion™, J. Kor. Phys. Soc. 73 (12) (2018) 1814–1820.
[19] S.-G. Crystals, BC-400, BC-404, BC-408, BC-412, BC-416 Premium Plastic Scintillators, Saint-Gobain Crystals, Nemours, 2005.
[20] E.J. Hall, A.J. Giaccia, Radiobiology for the Radiologist, Philadelphia, 2006.